

Effect of bend separation distance on the mass transfer in back-to-back pipe bends arranged in a 180° configuration

X. Chen¹ · T. Le² · D. Ewing² · C. Y. Ching²

Received: 21 January 2016 / Accepted: 5 February 2016 / Published online: 18 February 2016
© Springer-Verlag Berlin Heidelberg 2016

Abstract The mass transfer to turbulent flow through back-to-back pipe bends arranged in a 180° configuration with different lengths of pipe between the bends was measured using a dissolving gypsum test section in water. The measurements were performed for bends with a radius of curvature of 1.5 times the pipe diameter (D) at a Reynolds numbers of 70,000 and Schmidt number of 1280. The maximum mass transfer in the bends decreased from approximately 1.8 times the mass transfer in the upstream pipe when there was no separation distance between the bends to 1.7 times when there was a $1D$ or $5D$ length of pipe between the bends. The location of the maximum mass transfer was on the inner sidewall downstream of the second bend when there was no separation distance between the bends. This location changed to the inner wall at the beginning of the second bend when there was a $1D$ long pipe between the bends, and to the inner sidewall at the end of the first bend when there was a $5D$ long pipe between the bends.

List of symbols

ΔC_o	Initial concentration difference (g/l)
C_b	Bulk flow concentration (g/l)
C_w	Pipe wall concentration (g/l)
D_m	Gypsum diffusivity in water at 25 °C (m ² /s)
D	Pipe inner diameter (m)

e	Roughness height (m)
e/D	Relative roughness
e^+	Relative roughness scale
h	Mass transfer coefficient (m/s)
L	Length of pipes between pipe bends (m)
R_c	Pipe bend radius of curvature (m)
Re	Reynolds number
Sc	Schmidt number
Sh	Sherwood number
t	Experimental time (s)
x	Local distance along a pipe (m)
z	Streamwise distance from the start of the first pipe bend (m)
δ	Local instantaneous pipe surface wear (mm)
τ_m	Modified time (s)
ρ	Gypsum density (kg/m ³)
θ	Pipe circumferential angle (°)
ϕ	Angle along pipe bend (°)

Subscripts

1	First pipe bend
2	Second pipe bend
d	Downstream pipe
i	Intermediate pipe

1 Introduction

Flow-accelerated corrosion (FAC) is a corrosion and mass transfer process that results in metal loss in piping system components and equipment [1, 2]. The process results from the dilution of metallic ions (ferrous ions) into the fluid near the wall, some of which are transported to the bulk flow and some of which form oxides that are deposited on the wall forming a barrier to the dilution process. The metal

✉ C. Y. Ching
chingcy@mcmaster.ca

¹ School of Mechanical Engineering, Nanjing University of Science and Technology, Nanjing 210094, Jiangsu, People's Republic of China

² Department of Mechanical Engineering, McMaster University, Hamilton, ON L8S 4L7, Canada

removal rate depends on a number of factors, including the transport of the dissolved ions from the wall into the bulk flow and the transport of oxidants from the bulk flow to the near wall region. Thus, FAC is a concern near elements that cause large changes in the flow and promote turbulence and the transport of the ions between the wall region and the bulk flow [1, 2], and there is a need to characterize the mass transfer rates near these elements at high Schmidt numbers typical of ion transport in liquids.

The mass transfer in high Reynolds number turbulent flows through short radius 90° pipe bends, of interest here, is promoted on the inner wall near the bend inlet, on the side walls through the bend, and on the outer wall near and downstream of the bend exit [3–5]. The mass transfer is largest on the outer wall downstream of the bend exit; however, the enhancement relative to the mass transfer in the upstream pipe is also significant at other locations [5]. The mass transfer enhancement in pipe bends is affected by the radius of curvature of the bend [6–8] and can be related to the secondary flow within the bend. The secondary flow consist of a pair of mean counter-rotating motions [9, 10], though recent measurements indicate that the instantaneous secondary motion is a swirling mode that periodically switches direction [11, 12].

The mass transfer in bends is also affected by the proximity of other bends [13, 14]. The maximum mass transfer in short radius 90° pipe bends arranged in tandem in S and 90-degree-out-of-plane configurations occurs near the entrance of the second bend [13, 14], and the enhancement relative to the upstream pipe is significantly larger than that for a single 90° pipe bend. The mass transfer enhancement in these bends decreases when the length of pipe separating the bends increases. The location of maximum mass transfer also changes, particularly in the bends arranged in the 90-degree-out-of-plane configuration. The maximum mass transfer to high Reynolds number flows through short radius 180° bends appears to occur on the inner sidewalls of the second bend or downstream of it [8]. Heretofore, the effect that a length of pipe between the bends has on the mass transfer in back-to-back bends arranged in a 180° configuration has not been considered.

Poulson and Robinson [8] found that the mass transfer enhancement in 180° bends changed with Reynolds number. This was attributed to the development of roughness in the bend that was much larger than in the upstream pipe [8, 15]. The mass transfer at high Schmidt numbers, typical of FAC applications, is affected by even modest wall roughness [16, 17]. Thus, it is important to characterize the development of the roughness that occurs in dissolving wall mass transfer applications, such as FAC, where the roughness can develop on the surface as part of the mass transfer process.

The objective of this investigation is to examine the effect of bend proximity on the mass transfer in back-to-back pipe bends arranged in a 180° configuration. Measurements were performed for bends that were separated by pipes with lengths of 0, 1 and 5 diameters using a dissolving wall technique, with water flowing through cast gypsum test sections following [13, 14]. This process has a high Schmidt number, similar to that for the diffusion of the iron magnetite layer in carbon steel piping in water, providing a mass transfer environment analogous to FAC. The topography of the worn and unworn surfaces of the test sections are measured using a laser scanner so that the surface roughness and the local mass transfer over the entire surface can be characterized. The results show that the location and value of the maximum mass transfer enhancement changes with the proximity of the bends. The experiments were performed at a Reynolds number of 70,000 so that the results could be compared to the cases where the back-to-back bends were arranged in a S-shape [13] and in a 90° out of plane configuration [14]. The experimental facility and methodology are described in the next section, followed by the results of the experiments and the conclusions of the study.

2 Experimental methodology

The dissolving wall mass transfer experiments were performed in a 2.54 cm (1 in.) diameter (D) test facility shown schematically in Fig. 1 that was also used in [13, 14]. Water from a 50 L water tank is circulated through the test loop by a centrifugal pump. The flow rate is regulated using globe valves and measured using a turbine flow meter. The water flow passes through a flow conditioning section before entering a 152.4 cm ($60D$) long straight acrylic pipe upstream of the test section. The gypsum test sections were oriented horizontally and the flow exited the test section to a 38.1 cm ($15D$) long straight acrylic pipe before being directed to the reservoir through a flexible hose. The water temperature was measured in the reservoir and maintained at $25 \pm 0.5^\circ\text{C}$ using a cooling loop. An electrical conductivity probe was used to measure the conductivity of the water in the reservoir to determine the overall mass of gypsum dissolved into the water. The probe was calibrated off line before the experiments.

The gypsum test sections included an 20.3 cm ($8D$) long straight pipe upstream of the bends, two 90° pipe bends with radius of curvature of 3.81 cm ($R_c/D = 1.5$), and a 10.2 cm ($4D$) long downstream straight section. Test sections without a pipe between the bends and with 2.54 cm ($1D$) and 12.7 cm ($5D$) long straight pipes between the bends were considered. The test section had a nominal diameter of 2.54 cm throughout. The test sections were

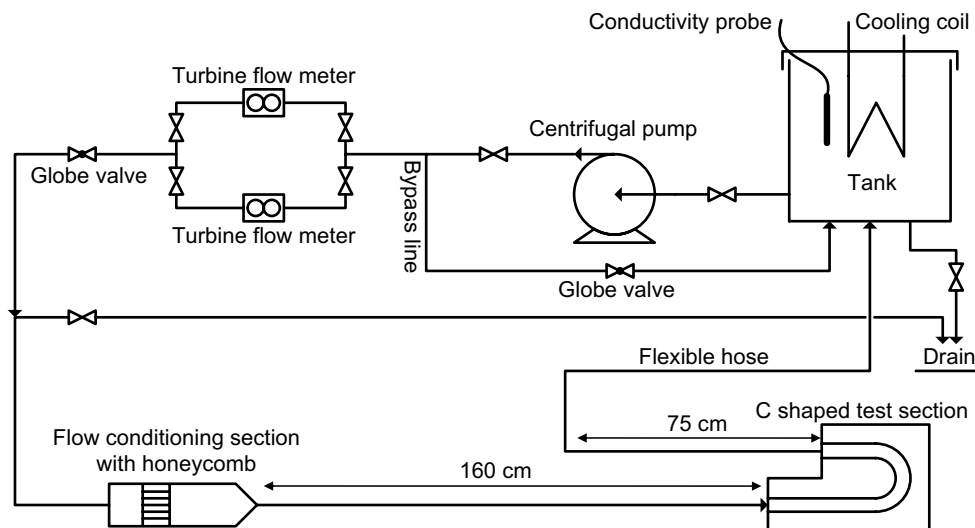


Fig. 1 Schematic showing the components of the test facility

cast from Hydrocal ($\text{CaSO}_4 \cdot 1/2 \text{H}_2\text{O}$) that produces high density Gypsum using solid molding cores that were held in position in an outer mold. The components were cast in succession so that the core could be removed from the different components. The cast test sections were then left to cure and dry until their weight reached a constant value using a scale accurate to ± 1 g. The test sections were also allowed to dry after each experiment until their weight was constant. The difference in the weight of the test section before and after each experiment was used as one measure of the overall mass removed during the experiment.

Once the test section from each experiment was dry, it was cut into two halves along the symmetry plane. This was also done for two unworn test sections that had not undergone testing. In each case, the surface topography of each half was measured relative to a common datum using a laser digitizer with a resolution of 0.2 mm. Several scans were taken from different directions to ensure complete surface coverage and increase the resolution of the data. The laser digitized surfaces were initially aligned to a common coordinate system using commercial software and then more precisely aligned and analyzed using in-house routines. The digitized data clouds were re-gridded to a uniform grid with nominal dimensions of 1.1° in the azimuthal direction and 0.5 mm ($0.02D$) along the pipe centerline. The section alignment was then refined based on the surface symmetry in the upstream and downstream pipe sections and checks were made for any systematic bias. The results in all cases were compared with the physical samples and the laser scanner results to ensure the surface was properly represented.

Mass transfer experiments for each test section configuration were performed multiple times over different time

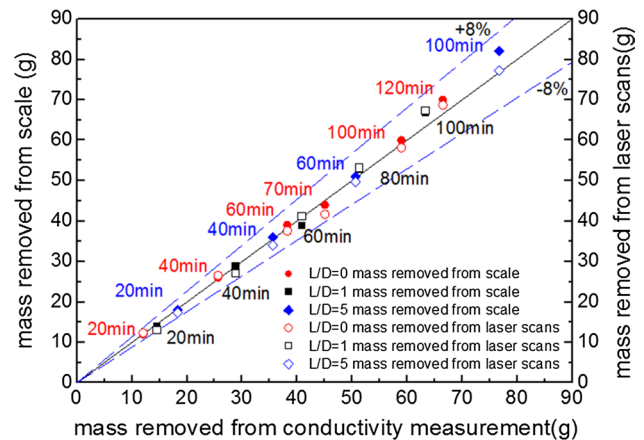


Fig. 2 Mass balance for the 180° pipe bends with $L/D = 0, 1$ and 5 for a Reynolds number of 70,000

periods from 20 to 120 min. A new test section was used at the start of each experiment. The local mass removed from each sample was determined by subtracting the local pipe radius of the worn sample from the local radius of the unworn sample that had not been tested. The overall mass removed from each sample was determined by integrating the local measurements. This was compared with the amount of mass removed from the difference in weight of the test section before and after the experiment and from the concentration of gypsum dissolved in the water during the experiment. The measured mass values agreed to within $\pm 8\%$ in all cases and well within this for the longer times as shown in Fig. 2.

Following [13, 14], the local mass transfer coefficient h was determined by

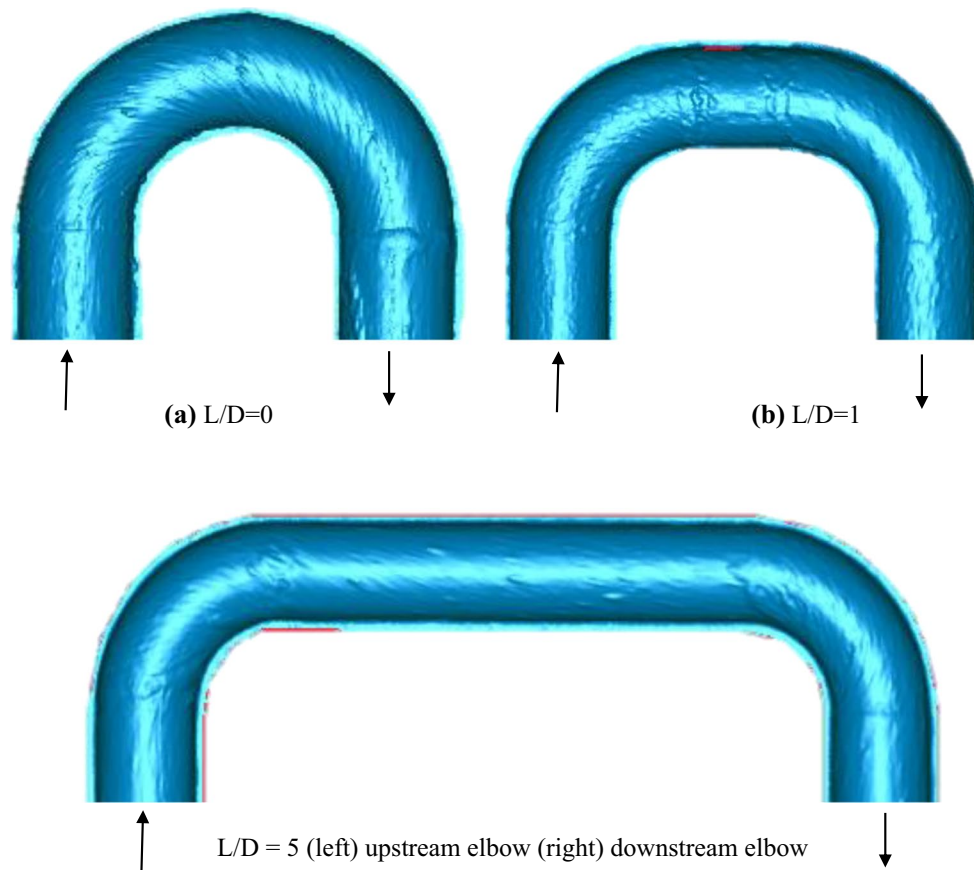


Fig. 3 Surface topologies of the bends after an experimental time of 60 min

$$\frac{\rho d\delta}{d\tau_m} = h\Delta C_o, \quad (1)$$

where δ is the local thickness of Gypsum removed, ρ is the Gypsum density and τ_m is a modified time given by

$$\tau_m = \frac{1}{\Delta C_o} \int_0^t (C_w - C_b) dt. \quad (2)$$

Here, C_w and C_b are the Gypsum concentration at the wall and in the bulk flow, respectively, and ΔC_o is the initial concentration difference. The modified time accounts for the change in the concentration difference between the wall and the bulk flow over the course of the experiment. The local rate at which the gypsum was removed ($d\rho\delta/d\tau_m$) was determined from a best linear fit to the data from the different samples run over the different experimental times. The gypsum concentration at the wall was taken as the saturation concentration for gypsum ions in water at 25 °C (2.4 g/L). The density of the gypsum was 1550 kg/m³. The resulting mass transfer coefficient h , is then used to compute the Sherwood number given by

$$Sh = \frac{hD}{D_m} \quad (3)$$

where D is the initial nominal pipe diameter and D_m is the mass diffusivity with a value of 6.5×10^{-10} m²/s at 25 °C. The measurements were performed for a Reynolds number of 70,000 where the Reynolds number is based on the initial nominal pipe diameter, and the Schmidt number is 1280. The nominal diameter of the upstream pipe increased approximately 4 % over the longest experimental time, and was considered in the uncertainty analysis. The uncertainty in the local Sherwood number estimated following [18] was approximately ± 23 %, while the uncertainty in the Reynolds number was ± 4 %.

3 Results and discussion

The analysis of the results was initiated by considering the roughness that developed on the surfaces of the test sections. Typical realizations of the surface in the bends and the pipes immediately upstream and downstream of the bends

are shown in Fig. 3. The results show evidence of round imperfections due to small air bubbles that were cast into the test section and imperfections at the seams due to imperfect bonding of the different components. The surfaces also have shallower narrow streaks caused by the flow over the surface. The streaks change direction through the bends and are thought to reflect the direction of the mean flow near the wall. The streaks are inclined relative to the bend centerline through the initial part of the first bend in all geometries as the secondary flow develops. The angle continues to change up to the end of the first bend when there was no separation between the bends ($L/D = 0$), but did not appear to change in the second bend consistent with flow measurements in 180° bends [19–22]. The angle of the streaks did not continue to change through the latter part of the first bend when there was a straight pipe between the bends. The streaks also became less inclined along the pipe between the bends in the geometry with the $L/D = 5$ pipe between the bends, likely because the strength of the secondary flow decreases downstream of the first bend. This decrease in angle is not evident in the geometry for the $L/D = 1$ case. However, the inclination of the streaks in the second bend are smaller than in the geometry with $L/D = 0$, indicating that the presences of the pipe does impact the secondary flow in the second bend.

The local surface roughness was examined by subtracting the local radius of the pipe from a running local average radius over a larger area (approximately 10° in the azimuthal direction and $0.2D$ along the centerline). A distribution of the roughness for the geometry with $L/D = 1$ is shown in Fig. 4. These results show evidence of the streaks and other roughness features. The size of the local roughness in the upstream pipe and in the bends was characterized by estimating the typical peak to valley height of the variations in each region. The change in this roughness with the testing period for the $L/D = 1$ case is shown in Fig. 5. The results show that roughness was present on the wall of the pipe and bends even at the end of the shortest experimental time. The size of the roughness increased with the testing period, though at a decreasing rate. The size of the roughness in the bends is larger than in the upstream pipe, similar to the results of [8], although there is roughness in the pipe in the present case. The size of the roughness was similar to that in back-to-back bends arranged in an out-of-plane configuration measured using the same approach [14], but smaller than the roughness for measurements in a single bend and bends arranged in an S-configuration [5, 13].

The effect of roughness on the mass transfer can be characterized by considering the results for flow through channels and pipes with regular roughness [16, 17]. Those results indicate that a surface should be hydraulically smooth when e^+ , the roughness Reynolds number (eu^*/ν), is less than approximately 3. The value of Sh_r/Sh_s , the ratio of the Sherwood number for the rough wall relative to

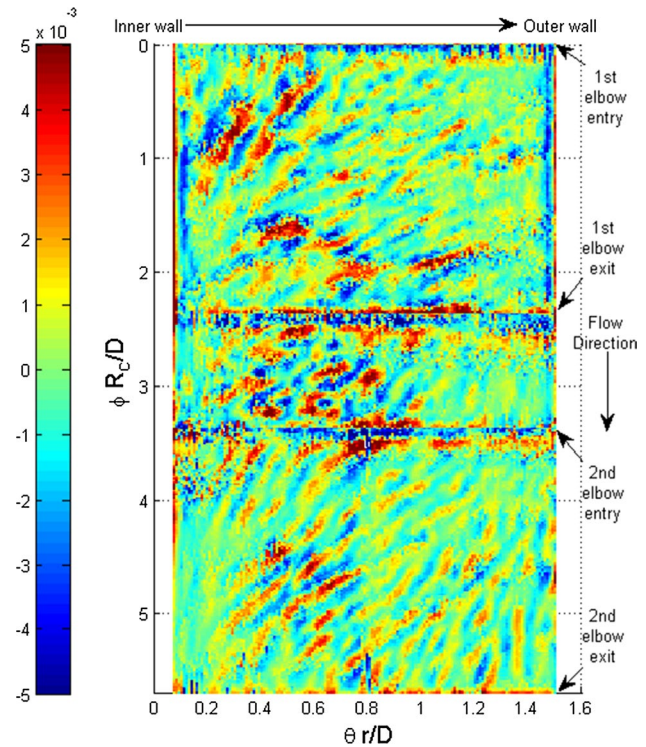


Fig. 4 Relative roughness on the surface with $L/D = 1$ after an experimental time of 120 min

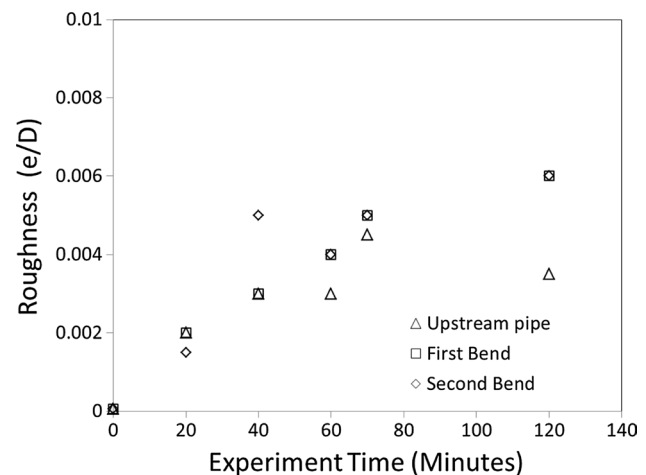


Fig. 5 Change in the relative roughness in the pipe and bends for $L/D = 1$ with time

that for a smooth wall, increases for e^+ between 3 and 10, reaching a maximum between e^+ of 10 to 15, and thereafter decreasing with e^+ [16, 17]. For fully developed pipe flow with a Reynolds number of 70,000, a value of e^+ of 10 corresponds to $e/D \sim 2.5 \times 10^{-3}$. The roughness in the pipe was larger than this in the pipe and bends after all but the shortest experimental time, and near this at this time.

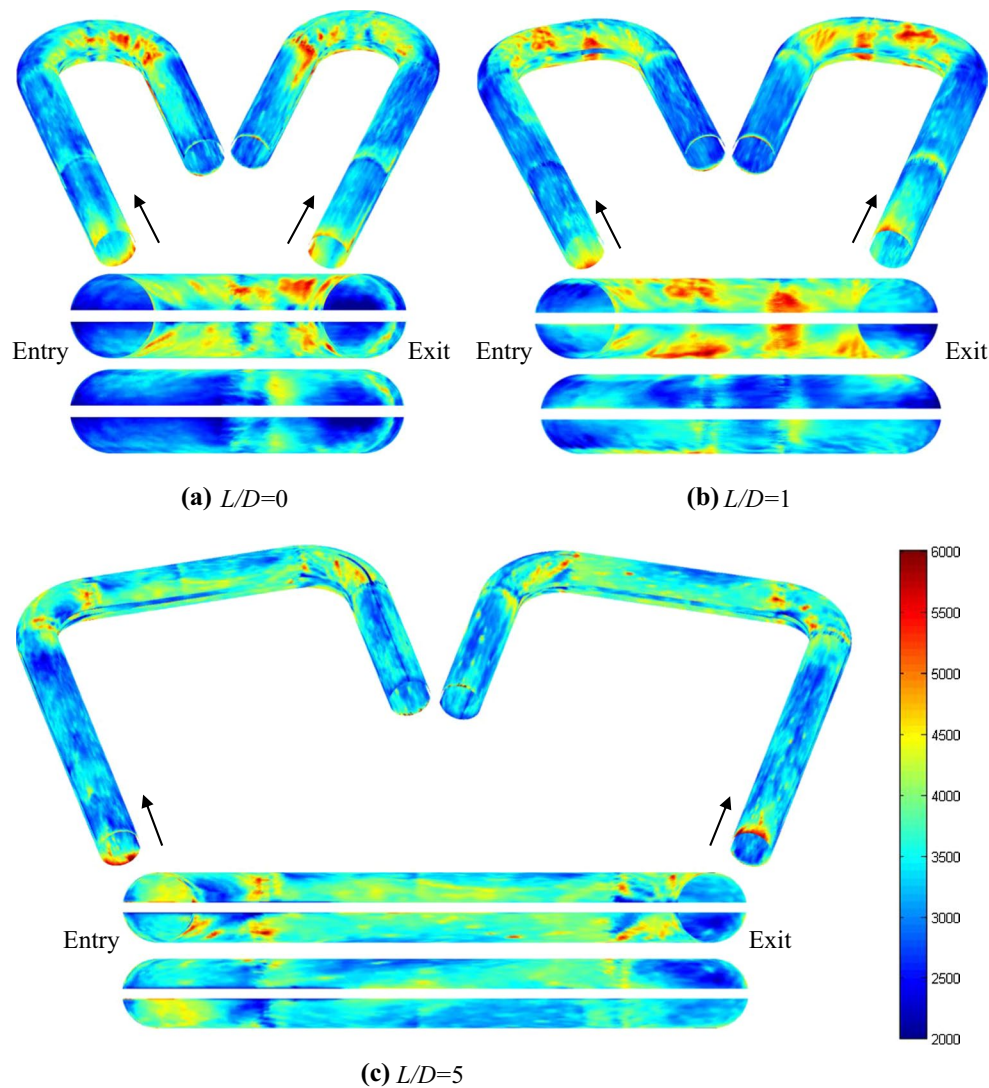


Fig. 6 Local Sherwood number contours for the 180° pipe bends with different separation distances for a Reynolds number of 70,000 and Schmidt number of 1280

The distribution of the local Sherwood number for the different geometries is shown in Fig. 6. The mass transfer rate appeared uniform and axisymmetric in much of the inlet pipe for the $L/D = 5$ case. The Sherwood number was elevated at the pipe inlet due to entrance effects. This persisted for approximately two diameters into the pipe. There was a second region of elevated Sherwood number in the inlet pipe for the geometries with $L/D = 0$ and 1. The inlet pipes for these test sections were cast in two sections and the mass transfer was elevated at the seam between the sections. The average Sherwood number in the pipe over a region from $1D$ to $3D$ upstream of the first bend varied between approximately 3050 and 3200, consistent with [5, 13, 14], and also consistent with the correlation for a rough pipe [23].

The Sherwood number in the first bend was elevated on the inner wall near the bend inlet in all the geometries.

There was also a region of elevated mass transfer on the sidewall of the first bend consistent with the results for the single bend [5]. The mass transfer in the geometry with $L/D = 0$ was elevated on the inner sidewall of the second bend and in the pipe immediately downstream of the second bend. The mass transfer in the geometry with $L/D = 1$ was elevated on the inner sidewall of the pipe immediately downstream of first bend and on the inner wall of the second bend at the bend inlet. The mass transfer was also elevated on the inner wall of the second bend though not as much as in the geometry without a pipe between the bends. The mass transfer in the geometry with $L/D = 5$ was elevated on the inner wall and inner sidewall of the pipe downstream of the first bend and on the inner wall of the second bend, though again not as much as in the $L/D = 0$ geometry.

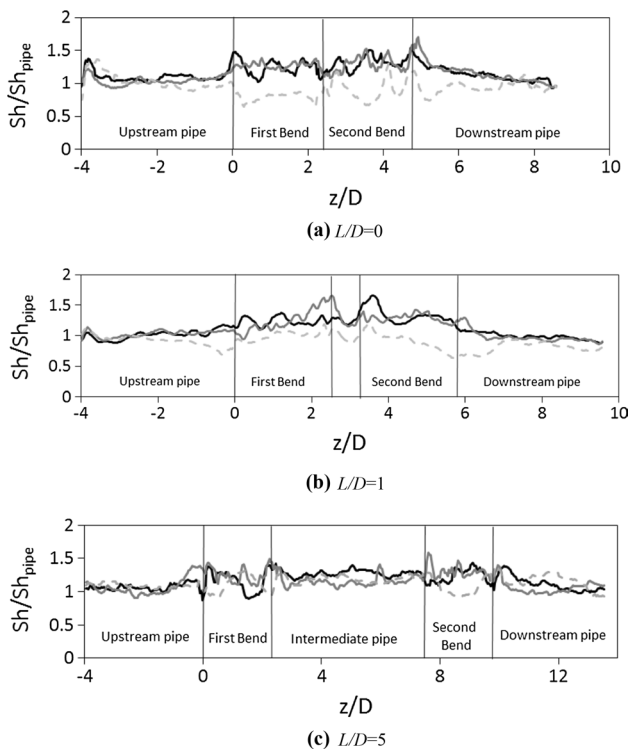


Fig. 7 Streamwise profiles of the mass transfer enhancement along the 180° pipe bend with $L/D = 0, 1$ and 5 for a Reynolds number of $70,000$ on the intrados at (black solid line) $\theta = 21^\circ$, (grey solid line) $\theta = 58^\circ$ and on the extrados at (grey dashed line) $\theta = 165^\circ$

Profiles of the mass transfer enhancement along the 180° bend and around the pipe circumference at different locations are shown in Figs. 7 and 8. The results here are the Sherwood number normalized by the Sherwood number from the corresponding upstream pipe. The position along the centerline z is measured relative to the start of the first bend, while the azimuthal position is measured relative to the inner radius with 180° corresponding to the outer radius. The distance x_i in the separation pipe is measured from the end of the first bend. The maximum mass transfer enhancement in the geometry with $L/D = 0$ of approximately 1.8 occurred in the first $0.3D$ downstream of the second bend at an azimuthal location between 40° and 75° from the inner radius of the bend. The maximum mass transfer enhancement in the geometry with $L/D = 1$ occurred in the first $0.3D$ of the pipe downstream of the first bend between 40° and 70° from the inner radius, and in the first $0.3D$ or 10° of the second bend at positions between 20° and 40° from the inner radius. The maximum mass transfer enhancement in both regions was approximately 1.7. The mass transfer enhancement was elevated in the second bend but the levels were smaller than in the pipe between the two bends. The maximum mass transfer for the geometry with the $L/D = 5$ was approximately 1.7

at locations between 40° and 70° from the inner radius near the end of the first bend.

The mass transfer enhancement in the 180° bend with $L/D = 0$ was well below the results from Poulson and Robinson [8] for small radius 180° bends at the Reynolds number of 70,000. Poulson and Robinson [8] reported that the maximum enhancement in this range of Reynolds number could be correlated by $0.71 Re^{0.12}$ that would yield a maximum enhancement of approximately 2.7 at a Reynolds number 70,000. Poulson and Robinson [8] argued that the change in the enhancement with Reynolds number was due to the fact that the wall in the bend was rough while the wall on the pipe was smooth. The maximum mass transfer enhancement of 1.8 found here with rough walls in the upstream pipe and bend, however, did agree with the value of 1.8 reported by Poulson and Robinson [8] for 180° bends with smooth walls in both the upstream pipe and bends. Thus, the results suggest that the mass transfer in the 180° bend may be approximately 1.8 times that observed in a pipe when the wall roughness conditions are similar.

The maximum mass transfer enhancement for the 180° bend is compared to the cases where the bends were arranged in a S-configuration [13] and a 90-degree out-of-plane configuration [14] in Fig. 9. The maximum mass transfer enhancement for the 180° configuration was substantially smaller than the maximum enhancements of 3.2 and 2.7 for the S-configuration [13] and 90° out-of-plane configuration [14] under the same conditions, with rough wall upstream pipes and bends. This value was even below the maximum enhancement of 1.85 downstream of a single 90° bend [5] with the same conditions. The mass transfer enhancement was smaller with the addition of the separation length between the bends. The maximum enhancements for the cases with $L/D = 1$ and 5 were similar to the local maximum mass transfer enhancement observed on the sidewalls of the single 90° bend [5]. The results for the individual bends in the 180° bend would be expected to recover to the results for the 90° bend as the separation distance between the bends increases. There was some mass transfer enhancement observed on the outer wall of the pipe in the geometry with $L/D = 5$, though not as much as that for the bends in the S- and out-of-plane configurations for the same length of pipe between the bends [13, 14], suggesting a further separation may be needed for this to occur. The reason for this is not clear and requires further investigation.

4 Summary and conclusion

The mass transfer in 180° bends with a radius of curvature of 1.5 time the pipe diameter and different lengths of pipe between the bends was measured at a nominal Reynolds

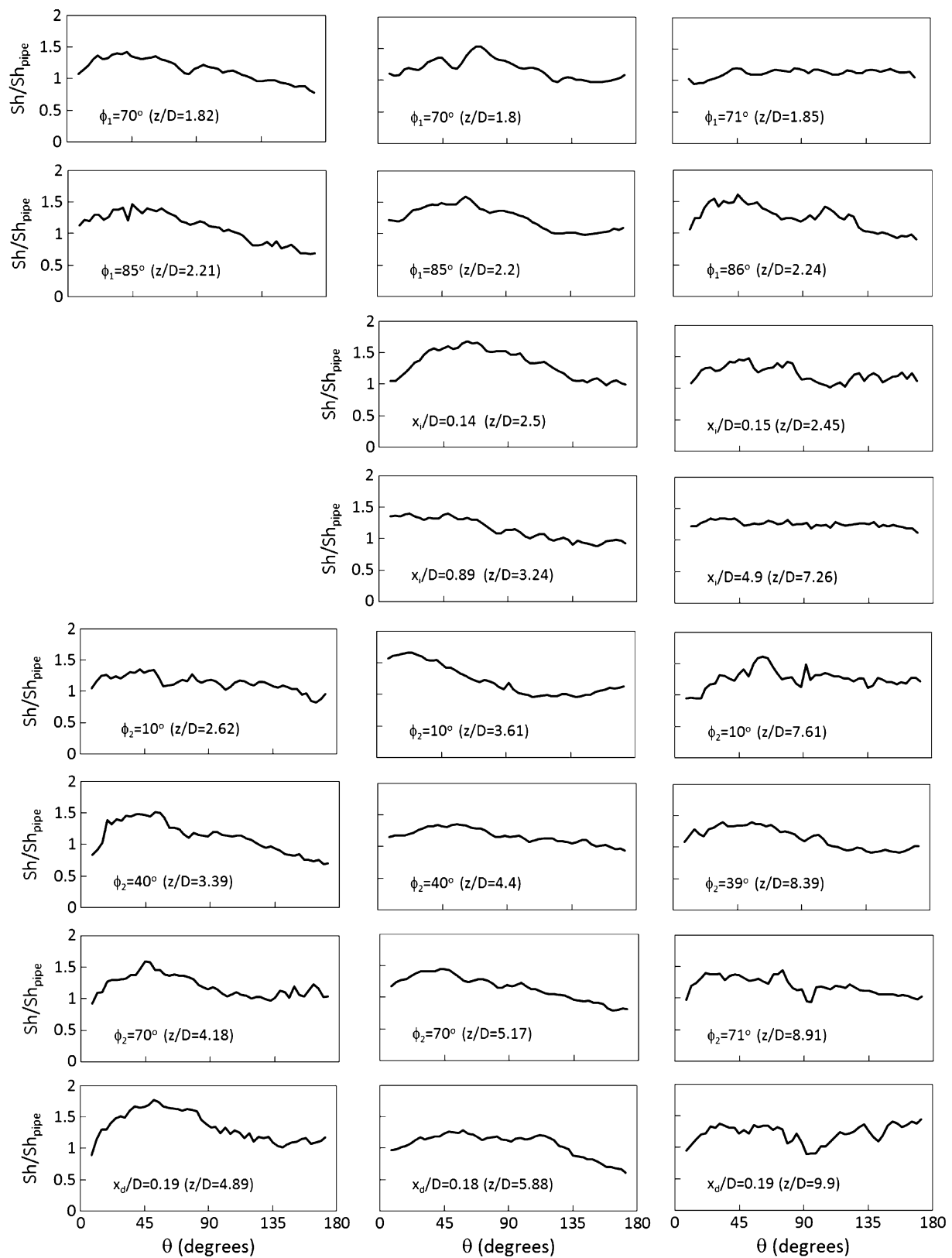


Fig. 8 Azimuthal profiles of the mass transfer enhancement for the 180° pipe bends with (left) $L/D = 0$, (center) $L/D = 1$ and (right) $L/D = 5$ for a Reynolds number of 70,000

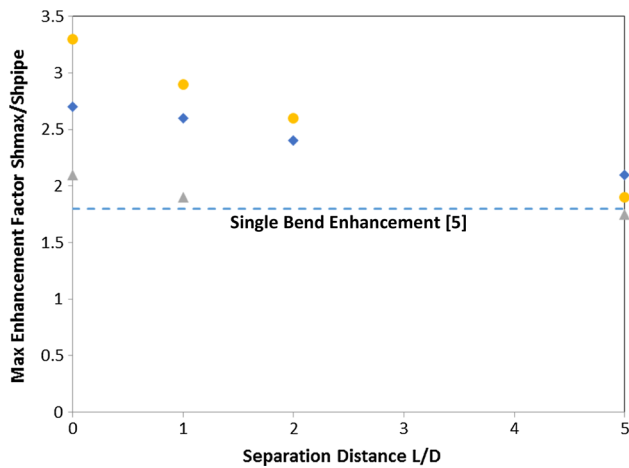


Fig. 9 Maximum enhancement factor in mass transfer for different elbow configurations with separation distance at Reynolds number of 70,000 for filled grey triangles 180° bend, filled blue diamond 90° out of plane bend [13] and filled yellow circle S-shape bend [14] (color figure online)

number of 70,000 and Schmidt number of 1280 using a dissolvable wall measurement technique. The results showed that the surface roughness of both the pipe and bends initially increased for small amount of mass removal, but changed more slowly as larger amounts of mass was removed. The roughness was larger in the bend than in the pipe, but appeared fully rough after short times in both regions. The local distributions of the Sherwood number over the surface showed that the mass transfer enhancement in the back-to-back bends was largest on the inner side wall near the end of the second bend when there was no separation distance between the bends. The location of the maximum enhancement was on the inner sidewall near the end of the first bend for the $L/D = 5$ geometry, and inner sidewall near the end of the first bend or the inner wall of the second bend inlet for the $L/D = 1$ geometry. The largest mass transfer enhancement relative to the mass transfer in the upstream pipe was approximately 1.8 when there was no separation between the bends. The maximum mass transfer enhancement in geometries with $L/D = 1$ and 5 was approximately 1.7, and slightly less than the mass transfer enhancement on the outer wall downstream of a single bend with the same radius of curvature. Thus, the results suggest the presence of the second bend in a 180° bend with moderate lengths of pipe between the bends changes the mass transfer distribution, but not necessarily the magnitude of the mass transfer enhancement relative to that in a single bend.

Acknowledgments The support of CANDU Owners Group (COG) and the Natural Sciences and Engineering Research Council of Canada (NSERC) is gratefully acknowledged.

References

- Uchida S, Naitoh M, Okada H, Suzuki H, Koikari S, Koshizuka S, Lister DH (2012) Key parameters to determine wall thinning due to flow accelerated corrosion. *ECS Trans* 25:77–90
- Pietralik JM (2012) The role of flow in flow-accelerated corrosion under nuclear power plant conditions. *E-J Adv Maint* 4:63–78
- Achenbach E (1976) Mass transfer from bends of circular cross section to air. *Future energy production systems*, vol 1. Academic Press, New York, pp 327–337
- Wilkin SJ, Oates HS, Coney MWE (1983) Mass transfer in straight pipes and 90° bends measured by the dissolution of plaster. Technology Planning and Research Division, Central Electricity Research Laboratories
- Mazhar H, Ewing D, Cotton JS, Ching CY (2013) Experimental investigation of mass transfer in 90° pipe bend using a dissolvable wall technique. *Int J Heat Mass Transf* 65:280–288
- Coney MWE (1981) Erosion corrosion: the calculation of mass transfer coefficients. *CEGB Rep RD L N 197:80*
- Sprague PJ, Patrick MA, Wragg AA, Coney MWE (1985) Mass transfer and erosion corrosion on pipe bends. In: *Proceedings 8th European Corrosion Conference*, Nice, vol I
- Poulson B, Robinson R (1988) The local enhancement of mass transfer at 180° bends. *Int J Heat Mass Transf* 31:1289–1297
- Tunstall MJ, Harvey JK (1968) On the effect of a sharp bend in a fully developed turbulent pipe-flow. *J Fluid Mech* 34(3):595–608
- Enayet MM, Gibson MM, Yianneskis M (1982) Laser Doppler measurements for laminar and turbulent flow in pipe bend. *Int J Heat Fluid Flow* 3:213–220
- Rutten F, Schroder W, Meinke M (2005) Large-eddy simulation of low frequency oscillations of the dean vortices in turbulent pipe bend flows. *Phys Fluids* 17:035107
- Hellstrom LHO, Zlatinov MB, Cao G, Smits AJ (2013) Turbulent pipe flow downstream of a 90° bend. *J Fluid Mech* 735:R7
- Mazhar H, Ewing D, Cotton JS, Ching CY (2014) Mass transfer in dual pipe bends arranged in an S-configuration. *Int J Heat Mass Transf* 71:747–757
- Le T, Ewing D, Schefski C, Ching CY (2014) Mass transfer in back to back bends arranged in an out of plane configuration. *Nucl Eng Des* 270:209–216
- Poulson B (1993) Advances in understanding hydrodynamic effects on corrosion. *Corros Sci* 35:655–665
- Dawson DA, Trass O (1972) Mass transfer at rough surfaces. *Int J Heat Mass Transf* 15:1317–1336
- Zhao W, Trass O (1997) Electrochemical mass transfer measurements in rough surface pipe flow: geometrically similar V-shaped grooves. *Int J Heat Mass Transf* 40:2785–2797
- Le T (2013) Mass transfer in back to back elbows arranged in an out of plane configuration under single & annular two-phase flow conditions. Master's Thesis, McMaster University, Hamilton, Canada
- Rowe M (1970) Measurements and computations of flow in pipe bends. *J Fluid Mech* 43(part 4):771–783
- Azzola J, Humphrey JAC, Iacovides H et al (1986) Developing turbulent flow in a U-bend of circular cross-section: measurement and computation. *J Fluids Eng* 108:214–221
- Sudo K, Sumida M, Hibara H (2000) Experimental investigation on turbulent flow through a circular-sectioned 180° bend. *Exp Fluids* 28:51–57
- Sugiyama H, Hitomi D (2005) Numerical analysis of developing turbulent flow in a 180° bend tube by an algebraic Reynolds stress model. *Int J Numer Methods Fluids* 47(12):1431–1449
- Postlethwaite J, Lotz U (1988) Mass transfer at erosion-corrosion roughened surfaces. *Can J Chem Eng* 66:75–78